

Lifted TASEP: a Bethe ansatz integrable paradigm for non-reversible Markov chains

Fabian H. L. Essler^{a,b} and Werner Krauth^b

^aRudolf Peierls Centre for Theoretical Physics, Clarendon Laboratory, Oxford OX1 3PU, UK; ^bLaboratoire de Physique de l'École normale supérieure, ENS, Université PSL, CNRS, Sorbonne Université, Université de Paris Cité, 24 rue Lhomond, 75005 Paris, France

This manuscript was compiled on June 23, 2023

Markov-chain Monte Carlo (MCMC), the field of stochastic algorithms built on the concept of sampling, has countless applications in science and technology. The overwhelming majority of MCMC algorithms are time-reversible and satisfy the detailed-balance condition, just like physical systems in thermal equilibrium. The underlying Markov chains typically display diffusive dynamics, which leads to a slow exploration of sample space. Significant speed-ups can be achieved by non-reversible MCMC algorithms exhibiting non-equilibrium dynamics, whose steady states exactly reproduce the target equilibrium states of reversible Markov chains. Such algorithms have had successes in applications but are generally difficult to analyze, resulting in a scarcity of exact results. Here, we introduce the “lifted” TASEP (totally asymmetric simple exclusion process) as a paradigm for lifted non-reversible Markov chains. Our model can be viewed as a second-generation lifting of the reversible Metropolis algorithm on a one-dimensional lattice and is exactly solvable by an unusual kind of coordinate Bethe ansatz. We establish the integrability of the model and present strong evidence that the lifting leads to faster relaxation than in the KPZ (Kardar–Parisi–Zhang) universality class.

Ever since its beginnings (1) in 1953, the field of Markov-chain Monte Carlo has relied on the concept of reversibility to sample probability distributions π in high-dimensional sample spaces Ω . Starting from an initial configuration x_0 , elements in the chain $x_0, x_1, \dots, x_t, x_{t+1} \dots$ sample π for large Monte-Carlo times t . In a reversible Markov chain at equilibrium (at large t), the chain link $\dots, x_t, x_{t+1}, \dots$ appears with the same probability as the time-reversed link $\dots, x_{t+1}, x_t, \dots$. The probability $P(x_t, x_{t+1})$ of a transition from x_t to x_{t+1} thus fulfils the famous detailed-balance condition $\pi_{x_t} P(x_t, x_{t+1}) = \pi_{x_{t+1}} P(x_{t+1}, x_t)$. Reversible Markov chains like the Metropolis (1) and the heatbath (2–4) algorithms mimic physical systems in thermal equilibrium, where all net flows vanish, so that the dynamics is diffusive and hence slow.

Markov chains need not be reversible, as a steady state π characterized by the “global-balance” condition $\pi_x = \sum_{y \in \Omega} \pi_y P_{yx}$ can be targeted without respecting detailed balance. The resulting non-reversible Markov chains can be viewed as out-of-equilibrium processes that approach the equilibrium distribution π for large t . Their non-vanishing flows often allow them to relax faster than diffusively. However, for many decades, genuinely non-reversible Markov chains that relax to a target equilibrium distribution were hard to construct. This changed with the advent of lifted Markov chains (5, 6).

Lifted Markov chains can be constructed from reversible chains as illustrated by the random walk on the lattice $\Omega^{\text{RW}} = \{1, \dots, L\}$ and its set of moves $\mathcal{L}^{\text{RW}} = \{-1, +1\}$ (see Methods for definitions). At each time $t = 0, 1, \dots$, a random move σ

(forward or backward) is applied to x_t and results in a new sample x_{t+1} :

$$\begin{array}{c} 1 \qquad \qquad \qquad L \\ \boxed{} \quad \boxed{} \quad \boxed{} \quad \boxed{} \\ \underbrace{\hspace{10em}}_{x_t \in \Omega^{\text{RW}}} \end{array} \rightarrow \begin{array}{c} \boxed{} \quad \boxed{} \quad \boxed{} \quad \boxed{} \\ \underbrace{\hspace{10em}}_{x_t \in \Omega^{\text{RW}}, \sigma \in \mathcal{L}^{\text{RW}}} \end{array} \rightarrow \begin{array}{c} \boxed{\bullet} \quad \boxed{} \quad \boxed{} \quad \boxed{} \\ \boxed{} \quad \boxed{} \quad \boxed{} \quad \boxed{} \\ \underbrace{\hspace{10em}}_{x_{t+1} \in \Omega^{\text{RW}}} \end{array} \quad \begin{array}{l} p = \frac{1}{2} \\ p = \frac{1}{2} \end{array} \quad [1]$$

Moves across the end points are rejected:

$$\begin{array}{c} 1 \qquad \qquad \qquad L \\ \boxed{\bullet} \quad \boxed{} \quad \boxed{} \quad \boxed{} \\ \underbrace{\hspace{10em}}_{x_t = 1 \text{ or } x_t = L} \end{array} \rightarrow \begin{array}{c} \boxed{} \quad \boxed{} \quad \boxed{} \quad \boxed{} \\ \underbrace{\hspace{10em}}_{\text{rejected back move}} \end{array} \rightarrow \begin{array}{c} \boxed{\bullet} \quad \boxed{} \quad \boxed{} \quad \boxed{} \\ \boxed{} \quad \boxed{} \quad \boxed{} \quad \boxed{} \\ \underbrace{\hspace{10em}}_{x_{t+1} \in \Omega^{\text{RW}}} \end{array} \quad \begin{array}{l} p = \frac{1}{2} \\ p = \frac{1}{2} \end{array} \quad [2]$$

The random walk is reversible with equal stationary probabilities $\pi^{\text{RW}}(x) = \frac{1}{L}$ for all x , but takes $\sim L^2$ moves to cover all L sites, signaling diffusive behavior.

The *lifted* random walk “duplicates” each $x_t \in \Omega^{\text{RW}}$ into an enlarged sample space $\Omega^{\text{L-RW}} = \Omega^{\text{RW}} \times \mathcal{L}^{\text{RW}}$

$$\begin{array}{c} \qquad \qquad \qquad i \\ \boxed{} \quad \boxed{} \quad \boxed{} \quad \boxed{} \\ \underbrace{\hspace{10em}}_{x_t \in \Omega^{\text{RW}}} \end{array} \rightarrow \begin{array}{c} (i, \sigma) \\ \boxed{} \quad \boxed{} \quad \boxed{} \quad \boxed{} \\ \boxed{} \quad \boxed{} \quad \boxed{} \quad \boxed{} \\ \underbrace{\hspace{10em}}_{x_t \in \Omega^{\text{L-RW}}} \end{array}, \quad [3]$$

which now contains $2L$ elements. In the bulk of the system, the lifted random walk first moves from (i, σ) to $(i + \sigma, \sigma)$, then, with probability $\alpha = 1 - \bar{\alpha}$, flips the direction from σ to $-\sigma$:

$$\begin{array}{c} \qquad \qquad \qquad i \\ \boxed{} \quad \boxed{} \quad \boxed{} \quad \boxed{} \\ \underbrace{\hspace{10em}}_{x_t \in \Omega^{\text{L-RW}}} \end{array} \xrightarrow{p=1} \begin{array}{c} \qquad \qquad \qquad i+\sigma \\ \boxed{} \quad \boxed{} \quad \boxed{} \quad \boxed{} \\ \underbrace{\hspace{10em}}_{x_{t+1} \in \Omega^{\text{L-RW}}, \alpha \ll 1, \bar{\alpha} = 1 - \alpha} \end{array} \rightarrow \begin{array}{c} \boxed{} \quad \boxed{} \quad \boxed{} \quad \boxed{} \\ \boxed{} \quad \boxed{} \quad \boxed{} \quad \boxed{} \\ \underbrace{\hspace{10em}}_{x_{t+1} \in \Omega^{\text{L-RW}}, \alpha \ll 1, \bar{\alpha} = 1 - \alpha} \end{array} \quad \begin{array}{l} p = \alpha \\ p = \bar{\alpha} \end{array}, \quad [4]$$

while at a boundary it may only flip σ :

$$\begin{array}{c} \qquad \qquad \qquad \\ \boxed{\bullet} \quad \boxed{} \quad \boxed{} \quad \boxed{} \\ \underbrace{\hspace{10em}}_{x_t \text{ at end point}} \end{array} \xrightarrow{p=1} \begin{array}{c} \qquad \qquad \qquad \\ \boxed{} \quad \boxed{} \quad \boxed{} \quad \boxed{} \\ \underbrace{\hspace{10em}}_{\sigma \rightarrow -\sigma} \end{array} \rightarrow \begin{array}{c} \boxed{\bullet} \quad \boxed{} \quad \boxed{} \quad \boxed{} \\ \boxed{} \quad \boxed{} \quad \boxed{} \quad \boxed{} \\ \underbrace{\hspace{10em}}_{x_{t+1} \in \Omega^{\text{L-RW}}} \end{array} \quad \begin{array}{l} p = \alpha \\ p = \bar{\alpha} \end{array} \quad [5]$$

The lifted random walk is non-reversible (the move from (i, σ) to $(i + \sigma, \sigma)$ cannot be reversed), but its steady state is the equal-probability mixture of all $2L$ lifted configurations. For $\alpha = 1/L$, it moves in $\sim L$ steps through the lifted lattice of $2L$ sites, much faster than the original random walk. The increased sampling speed in the augmented space $\Omega^{\text{L-RW}}$ also boosts the exploration of the original Ω^{RW} .

In the present work, we consider liftings of the Metropolis algorithm for hard spheres a one-dimensional lattice, which

is nothing but the symmetric simple exclusion process (SSEP) (7–9). We introduce a second-generation non-reversible lifting, the lifted TASEP (totally asymmetric simple exclusion process), that again speeds up the timescales on which sample space is explored. The lifted TASEP has two striking properties. First, it features non-local moves, yet it can be solved exactly by the Bethe ansatz. This allows us to compute exact eigenstates of the transition matrix for large system sizes. Our analysis suggests that it belongs to a new class of Bethe ansatz solvable models with relaxation rates that are faster than for the KPZ (Kardar–Parisi–Zhang) class. Second, as our construction is based on the lifting principle (5, 6), our model immediately generalizes to the continuum (10, 11). It also connects to lifted MCMC algorithms in higher dimensions (12, 13), and with smooth interactions (14, 15), which have been successfully applied in statistical mechanics (16, 17) and chemical physics (18).

Exclusion models: from the SSEP to the lifted TASEP

The SSEP implements the reversible Metropolis algorithm for indistinguishable hard spheres on an L -site lattice with periodic boundary conditions. A known non-reversible lifting of the SSEP (with periodic boundary conditions) is the much studied TASEP (19–24). Here we introduce a “second-generation” lifting of the SSEP by constructing a lifting of the TASEP. It implements the same strategy for shortening relaxation times as the lifted random walk discussed in the introduction.

Symmetric simple exclusion process. In the SSEP, configurations are described by the occupied sites $\{\dots, i, j, k, \dots\}$. At each time step, a randomly chosen active particle

$$\underbrace{\begin{array}{|c|c|c|} \hline \bullet & \bullet & \bullet \\ \hline \end{array}}_{x_t \in \Omega^{\text{SSEP}}} \rightarrow \left\{ \begin{array}{l} \begin{array}{|c|c|c|} \hline \bullet & \leftarrow \bullet & \bullet \\ \hline \end{array} & p = \frac{1}{N} \\ \begin{array}{|c|c|c|} \hline \bullet & \bullet & \leftarrow \bullet \\ \hline \end{array} & p = \frac{1}{N} \\ \begin{array}{|c|c|c|} \hline \bullet & \bullet & \bullet \\ \hline \end{array} & p = \frac{1}{N} \end{array} \right\} \rightarrow \dots, \quad [6]$$

choice of active particle

attempts a random forward or backward move:

$$\dots \rightarrow \underbrace{\begin{array}{|c|c|c|} \hline \bullet & \leftarrow \bullet & \bullet \\ \hline \end{array}}_{\text{choice of move}} \rightarrow \left\{ \begin{array}{l} \begin{array}{|c|c|c|} \hline \bullet & \bullet & \bullet \\ \hline \end{array} & p = \frac{1}{2} \\ \begin{array}{|c|c|c|} \hline \bullet & \bullet & \bullet \\ \hline \end{array} & p = \frac{1}{2} \end{array} \right\}. \quad [7]$$

$x_{t+1} \in \Omega^{\text{SSEP}}$

Moves that would violate the exclusion condition (at most one particle per site) are rejected, resulting in $x_{t+1} = x_t$. The SSEP is reversible and its steady state is the equal-probability mixture of all configurations $\pi_x = \text{const} \quad \forall x \in \Omega^{\text{SSEP}}$ (see Methods for examples). The relaxation time (see Methods) scales as $t_{\text{rel}}^{\text{SSEP}} \sim N^3$. In contrast, the approach towards equilibrium from a worst-case initial configuration takes place on a non-asymptotic (25) mixing time scale t_{mix} , which scales as $\sim N^3 \log N$, i.e. a factor $\log N$ larger than the relaxation time. The approach to equilibrium thus takes longer than the de-correlation in equilibrium, giving rise to the celebrated “cutoff phenomenon” (8, 9, 25), a sudden convergence towards π at $t \sim t_{\text{mix}}$.

Totally symmetric simple exclusion process. One possible lifting of the SSEP is the “bi-directional” TASEP, where the sample space is augmented $\Omega^{\text{TASEP}} = \Omega^{\text{SSEP}} \times \{-1, +1\}$ while the move set is reduced (see Methods for an example transition matrix of the bi-directional TASEP). For periodic boundary conditions we may restrict ourselves to the forward-moving sector. Then, at each time step $t = 0, 1, \dots$, a randomly chosen active particle

$$\underbrace{\begin{array}{|c|c|c|c|} \hline \bullet & \bullet & \bullet & \bullet \\ \hline \end{array}}_{x_t \in \Omega^{\text{TASEP}}} \rightarrow \left\{ \begin{array}{l} \begin{array}{|c|c|c|c|} \hline \bullet & \leftarrow \bullet & \bullet & \bullet \\ \hline \end{array} \rightarrow \begin{array}{|c|c|c|c|} \hline \bullet & \bullet & \bullet & \bullet \\ \hline \end{array} \\ \begin{array}{|c|c|c|c|} \hline \bullet & \bullet & \leftarrow \bullet & \bullet \\ \hline \end{array} \rightarrow \begin{array}{|c|c|c|c|} \hline \bullet & \bullet & \bullet & \bullet \\ \hline \end{array} \\ \begin{array}{|c|c|c|c|} \hline \bullet & \bullet & \bullet & \leftarrow \bullet \\ \hline \end{array} \rightarrow \begin{array}{|c|c|c|c|} \hline \bullet & \bullet & \bullet & \bullet \\ \hline \end{array} \end{array} \right\} \quad [8]$$

active particle $x_{t+1} \in \Omega^{\text{TASEP}}$

attempts a forward move, which is rejected if it violates the exclusion condition. The TASEP is non-reversible, and its steady state is the equal-probability mixture of all configurations (see Methods for an example). In the TASEP, both the relaxation time (20, 26) and the mixing time (27) scale as $t_{\text{rel}}, t_{\text{mix}} \sim N^{5/2}$, i.e. much faster than for the SSEP. The exponent $5/2$ reduces to $3/2$ if there are $\sim N$ moves per unit time (see Methods) which is characteristic of the KPZ universality class (28).

Lifted TASEP. In the lifted TASEP, a configuration is characterized by the positions of the particles, and in addition the identity of the active particle (and in principle its direction, see Methods). Restricting ourselves to the forward-moving sector, a lifted-TASEP configuration is denoted by $\{\dots, j, \vec{k}, l, \dots\}$ and refers to a three-state model, where sites are either empty, occupied with a “regular” article, or with the active particle, which is the only one that can move. Specifically, the deterministic first part of the move

$$\underbrace{\begin{array}{|c|c|c|c|} \hline \bullet & \vec{k} & \bullet & l \\ \hline \end{array}}_{x_t \in \Omega^{\text{L-TASEP}}} \rightarrow \underbrace{\begin{array}{|c|c|c|c|} \hline \bullet & \bullet & \vec{k+1} & l \\ \hline \end{array}}_{\text{“particle” displacement}} \xrightarrow{\text{Eq. [9]b}} \dots \quad [9]$$

$$\underbrace{\begin{array}{|c|c|c|c|} \hline \bullet & \vec{k} & k+1 & \bullet \\ \hline \end{array}}_{x_t \in \Omega^{\text{L-TASEP}}} \rightarrow \underbrace{\begin{array}{|c|c|c|c|} \hline \bullet & \bullet & \vec{k} & k+1 \\ \hline \end{array}}_{\text{“lifting” move}} \xrightarrow{\text{Eq. [10]b}} \dots \quad [10]$$

is complemented by a stochastic “pullback” with probability α , which transfers the “activity” from the active particle to the particle preceding it, without modifying the set of positions:

$$\dots \rightarrow \begin{array}{|c|c|c|c|} \hline \bullet & \vec{k} & k+1 & l \\ \hline \end{array} \rightarrow \left\{ \begin{array}{l} \begin{array}{|c|c|c|c|} \hline \vec{j} & \bullet & k+1 & l \\ \hline \end{array} & p = \alpha \\ \begin{array}{|c|c|c|c|} \hline \bullet & \bullet & \vec{k} & l \\ \hline \end{array} & p = \bar{\alpha} \end{array} \right\} \quad [9b]$$

$$\dots \rightarrow \begin{array}{|c|c|c|c|} \hline \bullet & \bullet & \bullet & \bullet \\ \hline \end{array} \rightarrow \left\{ \begin{array}{l} \begin{array}{|c|c|c|c|} \hline \bullet & \bullet & \bullet & \bullet \\ \hline \end{array} & p = \alpha \\ \begin{array}{|c|c|c|c|} \hline \bullet & \bullet & \bullet & \bullet \\ \hline \end{array} & p = \bar{\alpha} \end{array} \right\} \quad [10b]$$

$x_{t+1} \in \Omega^{\text{L-T}}$

The pullback can be very non-local, as for example in the move $\{\dots, j, \vec{k}, l, \dots\} \rightarrow \{\dots, \vec{j}, k+1, l, \dots\}$ of Eq. [9]b for $j \ll k$.

The non-zero row elements of the transition matrix $P^{\text{L-T}}$ can be read off from Eqs [9] and [10]. For $k+1 < l$, we have

$$\begin{aligned} P^{\text{L-T}}(\{\dots, j, \vec{k}, l, \dots\}, \{\dots, j, \vec{k+1}, l, \dots\}) &= \bar{\alpha}, \\ P^{\text{L-T}}(\{\dots, j, \vec{k}, l, \dots\}, \{\dots, \vec{j}, k+1, l, \dots\}) &= \alpha, \end{aligned} \quad [11]$$

while for $k + 1 = l$, the non-zero elements are

$$\begin{aligned} P^{L-T}(\{\dots j, \vec{k}, k+1 \dots\}, \{\dots j, k, \vec{k+1} \dots\}) &= \bar{\alpha}, \\ P^{L-T}(\{\dots j, \vec{k}, k+1 \dots\}, \{\dots j, \vec{k}, k+1 \dots\}) &= \alpha. \end{aligned} \quad [12]$$

In the above, periodic boundary conditions are understood. The two non-zero elements in Eqs [11] and [12] define the “ α ”-move and the “ $\bar{\alpha}$ ”-move out of the configuration $\{\dots j, \vec{k}, l \dots\}$. From these two equations, one may directly write down eigenvalue equations for the *right* eigenvectors of the transition matrix, namely, for $k + 1 > l$:

$$E\psi_{\{\dots j, \vec{k}, l \dots\}}^r = \alpha\psi_{\{\dots j, \vec{k}, k+1, l \dots\}}^r + \bar{\alpha}\psi_{\{\dots j, k, \vec{k+1}, l \dots\}}^r. \quad [13]$$

and for $k + 1 = l$:

$$E\psi_{\{\dots j, \vec{k}, k+1 \dots\}}^r = \alpha\psi_{\{\dots j, \vec{k}, k+1 \dots\}}^r + \bar{\alpha}\psi_{\{\dots j, k, \vec{k+1} \dots\}}^r. \quad [14]$$

Clearly, these are solved for $E = 1$ by $\psi^r = \text{const}$, so that P^{L-T} is a valid stochastic matrix with unit row sums. The transition matrix has non-zero diagonal elements (see Eq. [12]), so that it is aperiodic for any pullback $0 < \alpha < 1$. The non-zero *column elements* of the transition matrix are as follows.

For $j < k - 1$ and $l > k + 1$:

$$\begin{aligned} P^{L-T}(\{\dots j, \vec{k-1}, l \dots\}, \{\dots j, \vec{k}, l \dots\}) &= \bar{\alpha}, \\ P^{L-T}(\{\dots j, k, \vec{l-1} \dots\}, \{\dots j, \vec{k}, l \dots\}) &= \alpha. \end{aligned} \quad [15]$$

For $j = k - 1$ and $l > k + 1$:

$$\begin{aligned} P^{L-T}(\{\dots \vec{k-1}, k, l \dots\}, \{\dots j, \vec{k}, l \dots\}) &= \bar{\alpha}, \\ P^{L-T}(\{\dots k-1, k, \vec{l-1} \dots\}, \{\dots j, \vec{k}, l \dots\}) &= \alpha. \end{aligned} \quad [16]$$

For $j < k - 1$ and $l = k + 1$:

$$\begin{aligned} P^{L-T}(\{\dots j, \vec{k-1}, l \dots\}, \{\dots j, \vec{k}, l \dots\}) &= \bar{\alpha}, \\ P^{L-T}(\{\dots j, \vec{k}, l \dots\}, \{\dots j, \vec{k}, l \dots\}) &= \alpha. \end{aligned} \quad [17]$$

For $j = k - 1$ and $l = k + 1$:

$$\begin{aligned} P^{L-T}(\{\dots \vec{j}, k, l \dots\}, \{\dots j, \vec{k}, l \dots\}) &= \bar{\alpha}, \\ P^{L-T}(\{\dots j, \vec{k}, l \dots\}, \{\dots j, \vec{k}, l \dots\}) &= \alpha. \end{aligned} \quad [18]$$

The column elements of the transition matrix thus add up to one, so that P^{L-T} is in fact *doubly stochastic*. This implies that the steady state is the equal-probability mixture of all configurations for $0 < \alpha < 1$ and shows that the model is indeed a lifting of the TASEP. Furthermore, from any of these cases, one may directly write down eigenvalue equations $E\psi = \psi P^{L-T}$ for the *left* eigenvectors ψ of P^{L-T} , which we will further analyze using the Bethe ansatz. Again, $\psi = \pi = \text{const}$ is the left eigenvector with eigenvalue 1, as already follows from the double stochasticity.

The lifted TASEP differs from the integrable defect particle in the asymmetric exclusion process studied in Ref. (29) in two important ways. First, in our stochastic process only the defect particle (that is, the active particle) moves. Second, our dynamics is non-local because the stochastic pullback interaction acts between the closest particles, but they may be far separated in space.

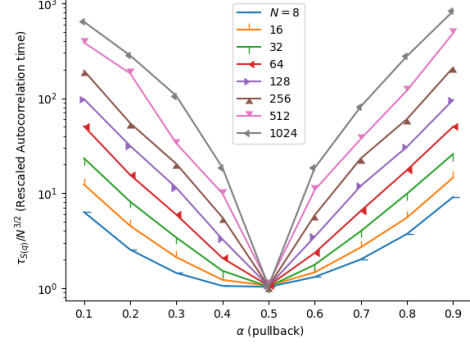


Fig. 1. Equilibrium autocorrelation time $\tau_{S(q)}$ for the structure factor $S(q)$ with $q = 2\pi/L$ (see Eq. [19]), as a function of the pullback α , for different system sizes.

Lifted TASEP: basic properties

While the value of the pullback $0 < \alpha < 1$ does not affect the steady state, it plays a remarkable role in the dynamics of the lifted TASEP. Any lifted configuration can evolve either through the “ α ”-move or the “ $\bar{\alpha}$ ”-move (see Eqs [11] and [12]). An $\bar{\alpha}$ -move advances the activity by one site. A series of $L - 1$ sequential $\bar{\alpha}$ -moves translates the entire configuration backwards by one site. An α -move, on average over all lifted configurations, pulls the activity back by $(L - N)/N$ sites. Averaging over α -moves and $\bar{\alpha}$ -moves shows that the activity drifts with velocity $-\alpha L/N + 1$, so that the drift velocity vanishes for $\alpha_{\text{crit}} = N/L$. In event-chain Monte Carlo, the drift velocity of the activity is proportional to the system pressure (15) and in the one-dimensional harmonic model, the zero-pressure point exhibits fast autocorrelation functions (30). This behavior was numerically confirmed in a continuous-space variant of the lifted TASEP (11) (see also Ref. (13)). Our pullback similarly generates a zero-pressure point at α_{crit} without affecting the steady-state properties.

MCMC simulations for the lifted TASEP confirm the special role of the pullback. We have analyzed the autocorrelation time $\tau_{S(q)}$ of the structure factor in equilibrium (31),

$$S(q, t) = \frac{1}{N} \left| \sum_{\xi \in \{\dots, i, j, k, \dots\}} e^{iq\xi} \right|, \quad [19]$$

where $q = 2\pi/L$ is the smallest wave number. The structure factor is sensitive to long-range density fluctuations, which are expected to relax slowly in equilibrium. As a function of α , $\tau_{S(q)}$ exhibits a pronounced dip at $\alpha = \alpha_{\text{crit}}$ (see Fig. 1).

At fixed α , we observe a power-law behavior of $\tau_{S(q)}$ as a function of N , but with different exponents at α_{crit} and away from it (see also Ref. (11)). Taking $L = 2N$ we find that for $\alpha = \alpha_{\text{crit}} = \frac{1}{2}$, these equilibrium autocorrelations are compatible with $\tau_{S(q)} \sim N^{3/2}$, while for non-critical $\alpha \in \{0.3, 0.4, 0.6, 0.7\}$, we observe $\tau_{S(q)} \sim N^{5/2}$ (see Fig. 2). At α_{crit} , the motion of the activity is driftless but superdiffusive (see also Ref. (11)): it only takes $\sim L^{3/2}$ steps for the activity to move through the system of L sites.

To estimate the mixing time t_{mix} for $\alpha = \alpha_{\text{crit}} = \frac{1}{2}$, we have taken the compact state $x_{t=0} = \{\vec{1}, 2, \dots, N\}$ as our conjectured worst-case initial configuration, and computed in a numerically exact way the total variation distance from the

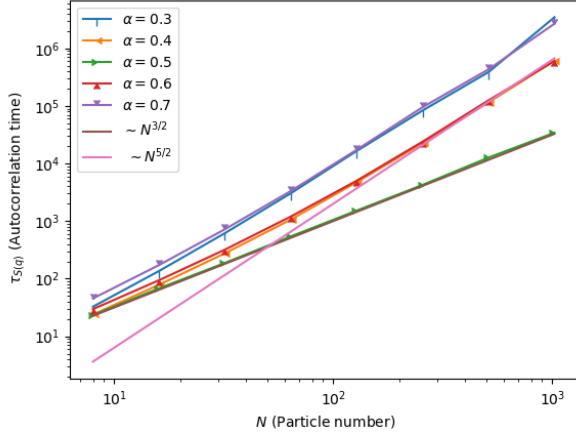


Fig. 2. Equilibrium autocorrelation time $\tau_{S(q)}$ for the structure factor $S(q)$ with $q = 2\pi/L$, as a function of $N = L/2$, for different values of the pullback.

steady state π (see Methods). Our data are compatible with $t_{\text{mix}} \sim N^2$. This is a clear indication that the lifted TASEP mixes much faster than the TASEP and does not belong to the KPZ universality class. We note again that, in our time units, the KPZ exponent is $5/2$. We have also estimated the diameter (the minimal time to connect any two configuration $x, y \in \Omega^{L\text{-TASEP}}$) appears to scale as $\sim N^2$ with a coefficient close to one (see Fig. 3).

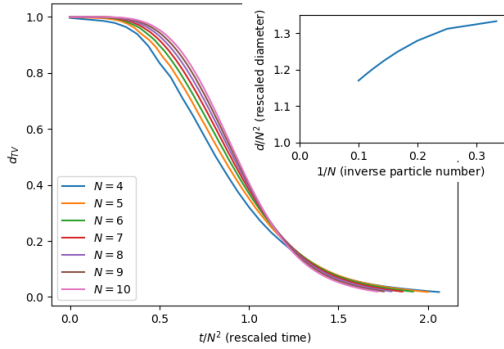


Fig. 3. Worst-case total variation distance d_{TV} for the lifted TASEP as a function of rescaled time t for small system sizes with $L = 2N$, at pullback $\alpha = \alpha_{\text{crit}} = \frac{1}{2}$. Inset: Diameter of the lifted TASEP, compatible with a scaling $\sim N^2$.

Spectrum of the transition matrix. To illustrate the spectrum of the transition matrix P^{L-T} and its dependence on the pullback α , we show in Fig. 4 the complex eigenvalues for $N = 4, L = 8$ as functions of α .

For $L = 2N$ and $\alpha = 0$, the $N \binom{2N}{N}$ eigenvalues lie on $2N(2N - 1)$ equally spaced points on the complex unit circle. Each of these eigenvalues has degeneracy

$$C(N - 1) = N \binom{2N}{N} / [2N(2N - 1)],$$

where C is the Catalan number. For $\alpha = 1$, the eigenvalues lie on $2N^2$ equally spaced points on the complex unit circle, and

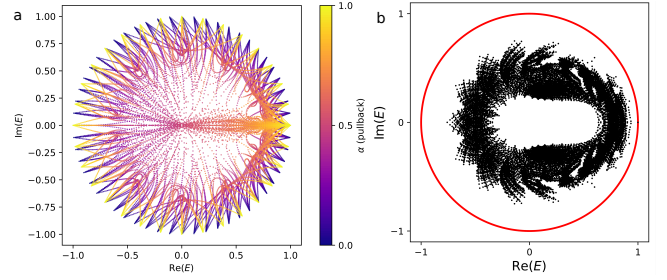


Fig. 4. Eigenvalue spectrum of the lifted TASEP. (a): Spectrum for $N = 4, L = 8$ as a function of the pullback α . For $\alpha = 0$ and 1 , all eigenvalues E are equally spaced on the complex unit circle. (b): Spectrum for $N = 7, L = 14$ for $\alpha = \alpha_{\text{crit}} = \frac{1}{2}$, with a single eigenvalue on the complex unit circle.

all the eigenvalues except $E = (1, 0)$ are again $C(N - 1)$ times degenerate, while the eigenvalue $E = (1, 0)$ has a degeneracy of $\binom{2N}{N} - (2N^2 - 1)C(N - 1)$ (see Fig. 4a). Clearly, in these two cases, the transition matrix P^{L-T} is not irreducible (except for $N = 2, \alpha = 0$), and it is periodic for all N . In contrast, for $0 < \alpha < 1$, the transition matrix P^{L-T} has only a single eigenvalue with $|E| = 1$ and is irreducible and aperiodic (see Fig. 4b).

Lifted TASEP: Bethe ansatz solution

In order to solve the eigenvalue equation for the transition matrix in the N -particle sector we introduce the following compact notations

$$\{j; a\} = \{j_1, \dots, j_{a-1}, \vec{j}_a, j_{a+1}, \dots, j_N\}. \quad [20]$$

Here, $j_1 < \dots < j_N$ are the positions of the N particles, and a specifies the active particle. The transition matrix of the lifted TASEP Eq. [18] then takes the form

$$\begin{aligned} P^{L-T}(\{k; b\}, \{j; a\}) = & \bar{\alpha} \delta_{a,b+1} \delta_{k_b+1, k_{b+1}} \delta_{j,k} \\ & + \bar{\alpha} \delta_{b,a} (1 - \delta_{k_b+1, k_{b+1}}) \delta_{j, k+e_b} \\ & + \alpha \delta_{b,a+1} (1 - \delta_{k_b+1, k_{b+1}}) \delta_{j, k+e_b} \\ & + \alpha \delta_{b,a} \delta_{k_b+1, k_{b+1}} \delta_{k,j}. \end{aligned} \quad [21]$$

Here we have defined $e_a = (0, \dots, 0, 1, 0, \dots)$, where the non-zero entry is at position a and $\delta_{j,k} = \prod_{n=1}^N \delta_{j_n, k_n}$. The left eigenvalue equation for P^{L-T} then takes the form

$$\begin{aligned} E \psi_a(j) = & \bar{\alpha} \psi_{a-1}(j) \delta_{j_a, j_{a-1}+1} \\ & + \bar{\alpha} \psi_a(\dots, j_a - 1, \dots) (1 - \delta_{j_a, j_{a-1}+1}) \\ & + \alpha \psi_{a+1}(\dots, j_{a+1} - 1, \dots) (1 - \delta_{j_{a+1}, j_a+1}) \\ & + \alpha \psi_a(j) \delta_{j_{a+1}, j_a+1}. \end{aligned} \quad [22]$$

As mentioned, when viewed as a non-Hermitian quantum spin chain (32), this corresponds to a three-state model with infinite-range interactions (see Methods). We solve the eigenvalue equation [22] by applying a nested Bethe ansatz

$$\psi_a(j) = \sum_{Q \in S_N} A_a(Q) \prod_{j=1}^N (z_j)^{j Q_j}, \quad [23]$$

where S_N is the set of all permutations of $(1, \dots, N)$ and $\{z_1, \dots, z_N\}$ are complex spectral parameters that specify a given solution. We note in passing that we have not attempted

to use the Bethe ansatz to determine the right eigenvectors of the transition matrix, which in general differ from the left eigenvectors but have the same eigenvalues. Substituting the Ansatz of Eq. [23] into Eq. [22] for the probabilities and assuming that $|j_n - j_{n-1}| > 1 \forall n$, we obtain

$$A_a(Q) \left[E - \frac{\bar{\alpha}}{z_{Q_a^{-1}}} \right] = \frac{\alpha}{z_{Q_{a+1}^{-1}}} A_{a+1}(Q) . \quad [24]$$

These relations express all $A_a(Q)$ in terms of only $A_1(Q)$

$$A_a(Q) = \left[\prod_{b=1}^{a-1} \frac{z_{Q_{b+1}^{-1}}}{\alpha} \left(E - \frac{\bar{\alpha}}{z_{Q_b^{-1}}} \right) \right] A_1(Q) . \quad [25]$$

Additional relations are obtained by considering ‘‘sector boundaries’’

(i) $\underline{j_{a-1} + 1 < j_a = j_{a+1} - 1}$. Here, the eigenvalue equation

$$E\psi_a(\mathbf{j}) = \alpha\psi_a(\mathbf{j}) + \bar{\alpha}\psi_a(\dots, j_a - 1, \dots) , \quad [26]$$

implies the following relations between amplitudes

$$\frac{A_a(C_a(Q))}{A_a(Q)} = \frac{z_{Q_{a+1}^{-1}}}{z_{Q_a^{-1}}} T(z_{Q_{a+1}^{-1}}, z_{Q_a^{-1}}) ,$$

$$T(z_1, z_2) = -\frac{E - \alpha - \bar{\alpha}/z_2}{E - \alpha - \bar{\alpha}/z_1} , \quad [27]$$

where $C_a(Q) = (\dots Q_{a+1}^{-1}, Q_a^{-1}, \dots)^{-1} = (a, a+1)Q$ is the permutation obtained from Q by swapping a with $a+1$. These can be rewritten as conditions on $A_1(Q)$ using Eq. [25]:

$$\frac{A_1(C_a(Q))}{A_1(Q)} = T(z_{Q_{a+1}^{-1}}, z_{Q_a^{-1}}) \begin{cases} 1 & \text{if } a > 1 , \\ \frac{z_{Q_{a+1}^{-1}}}{z_{Q_a^{-1}}} & \text{if } a = 1 . \end{cases}$$

(ii) $\underline{j_{a-1} + 1 = j_a < j_{a+1} - 1}$. Here, the eigenvalue equation

$$E\psi_a(\mathbf{j}) = \bar{\alpha}\psi_{a-1}(\mathbf{j}) + \alpha\psi_{a+1}(\dots, j_{a+1} - 1, \dots) \quad [28]$$

implies the following relations between amplitudes

$$\frac{A_a(C_{a-1}(Q))}{A_a(Q)} = -\frac{E - \alpha - \bar{\alpha}/z_{Q_{a-1}^{-1}}}{E - \alpha - \bar{\alpha}/z_{Q_a^{-1}}} \frac{E - \bar{\alpha}/z_{Q_a^{-1}}}{E - \bar{\alpha}/z_{Q_{a-1}^{-1}}} . \quad [29]$$

These can be rewritten as conditions on $A_1(Q)$ using Eq. [25]

$$\frac{A_1(C_{a-1}(Q))}{A_1(Q)} = T(z_{Q_a^{-1}}, z_{Q_{a-1}^{-1}}) , \quad a \geq 2 . \quad [30]$$

As an arbitrary permutation can be generated from the transpositions $(a, a+1)$ the conditions of Eqs [28] and [30] allow us to relate all amplitudes $A_1(Q)$ to $A_1(1, \dots, N)$. The various relations are equivalent to the following: let Q and Q' be two permutations related by a single transposition

$$Q' = \Pi_{t_1, t_2} Q , \quad [31]$$

where Π exchanges the entries Q_{t_1} and Q_{t_2} and we choose conventions such that we always have $Q_{t_1} < Q_{t_2}$. Then we have

$$\frac{A_1(Q)}{A_1(Q')} = T(z_{t_1}, z_{t_2}) \times \begin{cases} \frac{z_{t_1}}{z_{t_2}} & \text{if } 1 \in \{Q_{t_1}, Q_{t_2}\} \\ 1 & \text{else.} \end{cases} \quad [32]$$

The first case can be viewed as a scattering process between the active particle and an ordinary particle, while the latter corresponds to a scattering process involving two ordinary particles.

All conditions arising from other sector boundaries (e.g. three neighboring particles) reduce to Eqs [25] and [32].

Periodic boundary conditions. The periodic boundary conditions impose that

$$\psi_N(j_1, \dots, j_{N-1}, L+1) = \psi_1(1, j_1, \dots, j_{N-1}) ,$$

$$\psi_1(0, j_2, \dots, j_N) = \psi_N(j_2, \dots, j_N, L) . \quad [33]$$

They give rise to equations that determine the spectral parameters z_j and the eigenvalue E

$$z_a^{L-1} = \frac{\bar{\alpha}/z_a - E}{\alpha} \prod_{b=1}^N T(z_a, z_b) , \quad a = 1, \dots, N ,$$

$$\prod_{j=1}^N (E - \bar{\alpha}/z_j) = \alpha^N \prod_{k=1}^N \frac{1}{z_k} . \quad [34]$$

Explicit diagonalization of P^{L-T} for $N \leq 7$ and $L = 2N$ confirms the validity of these equations to machine precision.

Spectral properties of the lifted TASEP from the Bethe ansatz

The spectrum of the logarithm of the transition matrix $\ln(P^{L-T})$ can be determined for large system sizes by analyzing the Bethe equations [34]. Of particular interest are the steady state π and the ‘‘excitation gap’’, by which we denote the real part of the eigenvalue of $\ln(P^{L-T})$ closest to zero (cf Methods, Eqs [53] and [54]).

For simplicity, we again focus on the case $L = 2N$, so that $\alpha_{\text{crit}} = 1/2$. It is convenient to reparametrize the Bethe equations using

$$\beta = \frac{\bar{\alpha}}{E - \alpha} , \quad u_a = \frac{2z_a}{\beta} - 1 , \quad \delta = \frac{\beta - \bar{\alpha}/\alpha}{\beta + \bar{\alpha}/\alpha} ,$$

$$\mu = \left(\frac{2}{\beta} \right)^L \frac{1 - \alpha(1 - \beta)}{2\alpha} \prod_{b=1}^N \frac{u_b - 1}{u_b + 1} . \quad [35]$$

This maps Eq. [34] onto

$$(1 - u_a^2)^{\frac{L}{2}} = -\mu(u_a + \delta) , \quad a = 1, \dots, \frac{L}{2} ,$$

$$\left(\frac{2\alpha}{1 - \alpha(1 - \beta)} \right)^{\frac{L}{2}} = \prod_{b=1}^{\frac{L}{2}} (u_b + \delta) . \quad [36]$$

These equations are similar to the ones of the TASEP with periodic boundary conditions in that the equations for u_a can be written as simple polynomial equations involving a self-consistently determined constant. However, there are two key differences:

1. The factor $u_a + \delta$ in the equation for u_a makes the roots lie on a non-trivial contour whereas, for the TASEP, they lie on a circle.
2. The eigenvalue E enters like a root of a nested Bethe equation rather than being a simple additive function of the roots.

Steady state. The steady state π , that by construction is the equal-probability mixture, has $E = 1$, which implies that

$$\beta = 1, \quad \delta = 2\alpha - 1. \quad [37]$$

Our equations for $L = 2N$ then become

$$\frac{(1 - u_a^2)^{\frac{L}{2}}}{u_a - 1 + 2\alpha} = -\frac{2^L}{2\alpha} \prod_{b=1}^{\frac{L}{2}} \frac{u_b - 1}{u_b + 1}, \quad a = 1, \dots, \frac{L}{2},$$

$$(2\alpha)^{\frac{L}{2}} = \prod_{b=1}^{\frac{L}{2}} (u_b - 1 + 2\alpha). \quad [38]$$

Clearly $u_a \rightarrow 1$ solves these equations and gives back π .

Excitation gap for $\alpha = \alpha_{\text{crit}}$. For simplicity, we fix $L = 4m + 2$ for integer m . We have identified the structure of solutions of the Bethe equations that give rise to low-lying excitations by considering small system sizes $L \leq 14$. We then follow such solutions for larger values of L . In particular, this leads us to consider the following solution of the Bethe equations [36]. Out of the $L + 2$ roots of

$$(1 - u^2)^{\frac{L+2}{2}} + \mu_L(u + \delta_L) = 0, \quad [39]$$

we select a set $\{\bar{u}_1, \dots, \bar{u}_{\frac{L}{2}}\}$ that fulfils

$$\frac{L}{2} \ln[\bar{u}_n - 1] + \frac{L}{2} \ln[-\bar{u}_n - 1] - \ln(-\mu_L) - \ln(\bar{u}_n + \delta_L) = 2\pi i I_n, \quad [40]$$

where

$$\{I_n\} = \left\{ -\frac{L-2}{4}, \dots, -1, 0, 1, \dots, \frac{L-2}{4} \right\}. \quad [41]$$

We find that the root distribution of the corresponding excited state is of the form shown in Fig. 5. The logarithm of the

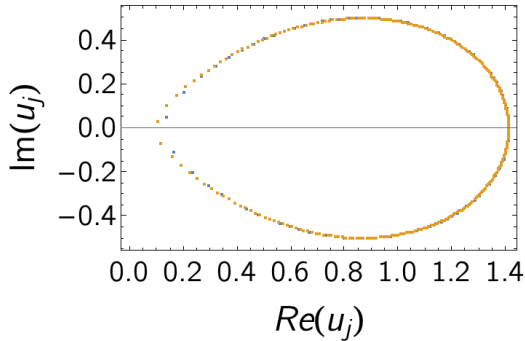


Fig. 5. Sets of roots $\{u_j | 1 \leq j \leq L/2\}$ corresponding to the excited state [41] for $L = 2N$ and $\alpha = \alpha_{\text{crit}} = \frac{1}{2}$, with $L = 214$ (blue) and $L = 494$ (yellow). For large L , the roots approach a non-trivial contour in the complex plane.

eigenvalue of these states is shown as a function of system size in Fig. 6. The numerical results are well described by a fit of the form

$$\ln[E_1(L)] = \frac{a_0}{L} + \frac{a_1}{L^{\frac{3}{2}}} + \frac{a_2}{L^2} + \frac{a_3}{L^{\frac{5}{2}}} + \frac{a_4}{L^3} + \mathcal{O}(L^{-\frac{7}{2}}), \quad [42]$$

where $a_0 = 6.284698i$, $a_1 = -0.047459i$, $a_2 = -20.0924 + 6.673286i$, $a_3 = 6.04464$ and $a_4 = -29.3419$. Interestingly, the real part of $\ln[E_1(L)]$ appears to scale as L^{-2} , while the

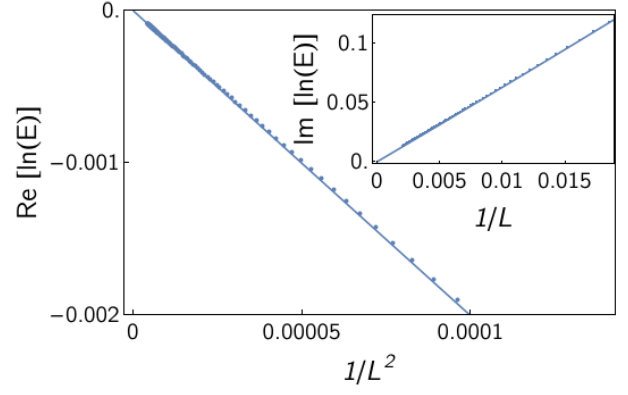


Fig. 6. Real and imaginary parts of the logarithm of the eigenvalue of the excited state [41] as functions of system size for $L = 2N$ and $\alpha = \alpha_{\text{crit}} = \frac{1}{2}$. The solid lines are fits described in the main text.

imaginary part scales as L^{-1} . Some comments are in order. The state Eq. [41] is the lowest excited state among those we have considered only for large L . This is unusual for Bethe-ansatz solvable models. Therefore, $\text{Re}(\ln[E_1(L)])$ is only an upper bound for the excitation gap.

Excitation gap for $\alpha \neq \alpha_{\text{crit}}$. For $L = 2N$, we have determined the scaling with system size of the eigenvalues of the solution specified by the same set of integers $\{I_n\}$ in Eq. [41] for several values of $\alpha \neq 1/2$. This again provides an upper bound of the excitation gap for large values of L . In Fig. 7 we show the root distributions for $\alpha = 0.3$, $\alpha = 0.4$ and $\alpha = 0.9$ respectively. The logarithm of the eigenvalue of these states is shown as a

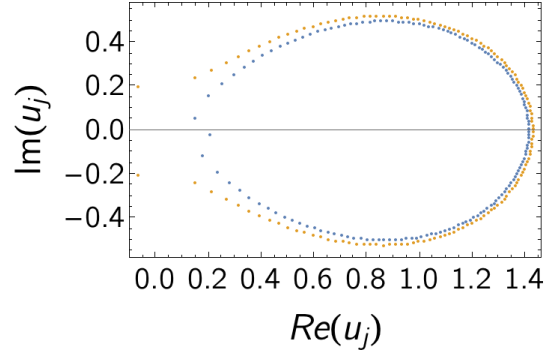


Fig. 7. Sets of roots $\{u_j | 1 \leq j \leq L/2\}$ corresponding to the excited state [41] for $\alpha = 0.9$, $N = L/2$ and $L = 272$ (yellow) and $\alpha = 0.4$, $N = L/2$ and $L = 290$ (blue).

function of system size in Fig. 8. Here we fit the excitation gap to the functional form

$$\text{Re}[\ln(E_1(L))] = \frac{a_0}{L^{\frac{5}{2}}} + \frac{a_1}{L^3} + \frac{a_2}{L^{\frac{7}{2}}} + \mathcal{O}(L^4),$$

$$\text{Im}[\ln(E_1(L))] = \frac{b_0}{L} + \frac{b_1}{L^{\frac{3}{2}}} + \frac{b_2}{L^2} + \mathcal{O}(L^{\frac{5}{2}}), \quad [43]$$

where for $\alpha = 0.4$, we find

$$a_0 = -573.913, \quad a_1 = 5651.58, \quad a_2 = -18183.4, \\ b_0 = -7.54557, \quad b_1 = 0.167695, \quad b_2 = -7.61005. \quad [44]$$

For $\alpha = 0.9$, the eigenvalue is real for all N , with

$$a_0 = -19.1347, \quad a_1 = 24.5024, \quad a_2 = -1.94545. \quad [45]$$

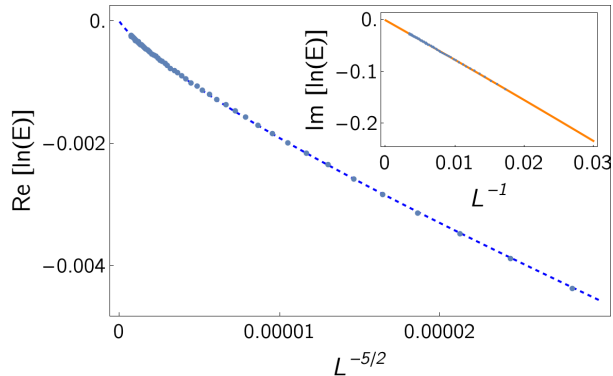


Fig. 8. Real part of the logarithm of the eigenvalue of the excited state described in the text for $\alpha = 0.4$ as functions of system size. The solid lines are fits described in the main text.

Discussion

Non-reversible lifted MCMC algorithms such as the lifted TASEP are all rooted in reversible Markov chains. In this paper, we have taken as our starting point the one-dimensional lattice reduction of the reversible hard-sphere Metropolis algorithm, which is nothing but the celebrated SSEP, itself a key paradigm for the stochastic dynamics of interacting particle systems.

The SSEP has been solved exactly and its mixing and relaxation times are known to scale differently with system size (8, 9). Its $t_{\text{rel}} \sim N^3$ scaling can be viewed as a particle diffusion in the Edwards–Wilkinson universality class (33). The scaling also follows from the proof (34) of the famous Aldous conjecture which identifies single-particle diffusion with the dynamics of exclusion models (35). We have constructed a second-generation lifting of the SSEP by inflating (“lifting”) each of its configurations $2N$ fold. Because liftings are by design local in space, it is known (6) that the maximal possible speedup (i.e. the reduction of mixing and relaxation time scales) scales at best with an exponent that is half the one of the base model. This corresponds to a diffusive-to-ballistic speed-up (36). The best-case inverse-gap scaling for liftings of the SSEP is $\sim N^{3/2}$ (up to multiplicative logarithms). Our MCMC simulations of the lifted TASEP are indeed compatible with this optimal scaling behavior for pullback $\alpha = \alpha_{\text{crit}}$: both the autocorrelation time $\tau_{S(q)}$ of the structure factor and the motion of the activity appear to scale a $N^{3/2}$. For $\alpha \neq \alpha_{\text{crit}}$, the same analysis suggests $\tau_{S(q)} \sim N^{5/2}$. In contrast, our simulations of the mixing time for a class of compact initial configurations suggests a scaling of $t_{\text{mix}} \sim N^2$ for $\alpha = \alpha_{\text{crit}}$.

As we have shown here, the lifted TASEP is exactly solvable by a nested Bethe ansatz in spite of its non-local structure. The Bethe equations derived in above yield exact information in particular on the spectrum of its transition matrix for large system sizes which are totally out of reach for other methods. Indeed, the analysis of these equations for specific families of numerically exact solutions with $L = 2N$ shows that the relaxation time cannot scale faster than $\sim N^2$ at α_{crit} and $\sim N^{5/2}$ for $\alpha \neq \alpha_{\text{crit}}$. While the latter agrees with our simulations of $\tau_{S(q)}$, the former is slower (but still much faster than for the SSEP or the TASEP). A possible explanation of this discrepancy is that $S(q)$ has for large N negligible overlap with the mode that gives rise to the $\sim N^2$ scaling of the inverse gap. We thus once again witness the exceptional difficulty of

estimating the timescales t_{mix} and t_{rel} in MCMC, even in the present simplified setting, and the utility of techniques such as the Bethe ansatz, which directly access the spectrum of the transition matrix.

Outlook. Our work raises a number of questions that should be addressed in future research. First and foremost, a more complete analysis of the spectrum of the transition matrix in the limit of large system sizes needs to be carried out, and the scaling behavior of the low-lying eigenvalues should be derived analytically by recasting the Bethe equations in terms of as nonlinear integral equations, cf. Refs (21, 37–39). Arguably the most important open question from the point of view of integrability is to determine the integrable structure of the lifted TASEP (its R-matrix and L-operator (40)). Given the spatially non-local nature of its transition matrix, it is not obvious how the lifted TASEP fits into the existing classification, and it would be interesting to clarify this. Knowing the integrable structure would be very helpful in addressing other pressing questions, like whether the partially asymmetric simple exclusion process has an integrable lifting as well, and which boundary conditions are compatible with integrability. This question is natural from the point of view of Monte-Carlo algorithms and also arises in the context of boundary-induced phase transitions in the TASEP. In particular one could ask whether there is a lifting of the open TASEP that reproduces its highly non-trivial steady state (41) but has a significantly shorter relaxation time. Another point that should be clarified is whether there is an integrable extension of our model to several active particles. Finally, we expect the continuum limit of the lifted TASEP at vanishing density (11) to be integrable.

Recent decades have witnessed the convergence of rigorous mathematical research on Markov chains and of the application-driven development of Monte Carlo algorithms. The present work proceeds further in this direction. The lifted TASEP, on the one hand, invites a mathematically rigorous analysis following in the footsteps of recent work on the TASEP and the SSEP. On the other hand, this new model is precisely the one-dimensional lattice reduction of the event-chain Monte Carlo algorithm, whose main applications to date have been in statistical and chemical physics. In this context, the Bethe ansatz has now entered the game as a powerful tool, in particular for analyzing complex spectra. The lifted TASEP is likely to be the first member of a larger class of integrable lifted Markov chains, and of non-reversible Monte Carlo algorithms relevant for applications in the sciences.

Materials and Methods

Markov chains. We here collect some basic definitions and results about Markov chains, lifted Markov chains, and Markov processes, and discuss the convergence towards the steady state.

Basic definition. We consider finite sample spaces Ω , and Markov chains defined by (i) a transition matrix P , where $P(x, y)$ gives the conditional probability to move in one time step to y if at x ; (ii) an initial distribution $\pi^{\{t=0\}}$, generally concentrated on a fixed initial configuration x_0 . The probability distribution at time $t = 1, 2, \dots$, starting from x_0 , is denoted by $\pi^{\{t\}} = P^t(x_0, \cdot)$. It satisfies $\pi_x^{\{t\}} = \sum_y \pi_y^{\{t-1\}} P(y, x)$. An irreducible Markov chain has a unique stationary solution that satisfies

$$\pi_x = \sum_{y \in \Omega} \pi_y P(y, x) \quad \forall x \in \Omega. \quad [46]$$

This equation becomes a condition on π , the ‘‘global balance’’ condition, in our case where the target distribution is imposed.

The steady state π is a row vector, and we refer to it as a left eigenvector of P with eigenvalue 1 (that is $E\pi = \pi P$, with $E = 1$). We call π an equal-probability mixture if all its elements are identical. For an irreducible Markov chain that is aperiodic (that is, has no periodicity in its return to a given configuration x), π is the limit of $\pi^{\{t\}}$ for $t \rightarrow \infty$. In the main text, we mention right eigenvectors, that is, column vectors ψ^r that satisfy $\psi^r = P\psi^r$, and in particular, the column vector $(1, \dots, 1)$, which indicates that the sum of the possibilities to move away from a configuration x (including back to x) must sum up to one. This means that the matrix is stochastic. The eigenvalue equation for left eigenvectors reads

$$E\psi_x = \sum_{y \in \Omega} \psi_y P(y, x) \quad \forall x \in \Omega. \quad [47]$$

For an irreducible and aperiodic transition matrix, the eigenvalue $E = 1$ is the only one with unit norm. The detailed-balance condition,

$$\pi_x P(x, y) = \pi_y P(y, x) \quad \forall x \in \Omega, y \in \Omega, \quad [48]$$

implies the global-balance condition, as follows from summing over y and using the conservation of probabilities $\sum_y P(x, y) = 1$. As discussed in the main text, detailed balance is equivalent to reversibility, whereas both the non-reversible and reversible Markov chain satisfy the global-balance condition Eq. [46].

Markov chains vs. Markov processes. In the main text, we consider discrete-time Markov chains where at $t = 0, 1, 2, \dots$, a single particle is displaced, modeling the computer implementation on a serial computer. The SSEP and the TASEP are usually defined as continuous-time Markov *processes*, where each of the elements of the respective move sets is sampled on average once per unit time. Thus, in the continuous-time SSEP, on average, $2N$ moves are attempted per unit time interval (N attempted moves for the continuous-time TASEP). The discrete-time and the continuous-time versions are bijections of each other, with a rescaling of time scales by a factor of $2N$ for the SSEP and a factor of N for the TASEP, and with the replacement of equidistant discrete time steps by Poisson-distributed ones. As a consequence the $\sim N^{5/2}$ relaxation and mixing-time scales of the discrete-time TASEP become $\sim N^{3/2}$ time scales in the continuous-time variant.

Lifted Markov chains. Lifting (5, 6) connects a Markov chain with sample space Ω , transition matrix P and steady state π with a lifted Markov chain $\hat{\Pi}$ with $\hat{\Omega}, \hat{P}, \hat{\pi}$ through a mapping f from $\hat{\Omega}$ to Ω . Under this transformation, π must be preserved,

$$\pi_v = \sum_{i \in f^{-1}(v)} \hat{\pi}_i,$$

where $f^{-1}(v)$ denotes the set of all $i \in \hat{\Omega}$ such that $f(i) = v$. In addition, the flows must be unchanged

$$\underbrace{\pi_v P(v, u)}_{\text{collapsed flow}} = \sum_{i \in f^{-1}(v), j \in f^{-1}(u)} \overbrace{\hat{\pi}_i \hat{P}(i, j)}^{\text{lifted flow}}.$$

In this paper, the lifted sample space $\hat{\Omega}$ is simply the Cartesian product of the ‘‘collapsed’’ sample space Ω with a space $\tilde{\mathcal{L}}$ of lifting variables, which correspond to the move set \mathcal{L} or parts of it ($\tilde{\mathcal{L}} \subset \mathcal{L}$). While the lifted sample space is thus enhanced, the set of moves is smaller, and the lifted transition matrix is sparser. Although the transition matrix and its lifted version are closely related, the mixing and relaxation times may be decreased (at most) to their square roots (6, 36).

Furthermore, in our case all the steady-state probabilities are constant, which implies that

$$P(v, u) = \frac{|\hat{\Omega}|}{|\Omega|} \sum_{i \in f^{-1}(v), j \in f^{-1}(u)} \hat{P}(i, j). \quad [49]$$

where $|\hat{\Omega}|$ denotes the size of the sample space $\hat{\Omega}$.

Convergence. For an irreducible and aperiodic Markov chain, $\pi^{\{t\}}$ converges towards π for $t \rightarrow \infty$ from any initial configuration x_0 . This convergence is commonly quantified by the worst-case distance $d_{\text{TV}}(t)$

$$d_{\text{TV}}(t) = \max_{x_0} \|P^t(x_0, \cdot) - \pi\|_{\text{TV}}, \quad [50]$$

where $\|\mu - \nu\|_{\text{TV}}$ denotes the total variation distance (TVD) between two distributions μ and ν :

$$\|\mu - \nu\|_{\text{TV}} = \frac{1}{2} \sum_{i \in \Omega} |\mu_i - \nu_i|. \quad [51]$$

The mixing time $t_{\text{mix}}(\epsilon)$ (which is known for the SSEP and the TASEP, and which we determine using numerical methods for the lifted TASEP). It is defined as the earliest time at which $d_{\text{TV}}(t) = \epsilon$, and satisfies $d_{\text{TV}}[t_{\text{mix}}(\epsilon)] \leq (2\epsilon)^\ell$ for $\ell = 1, 2, \dots$. This yields a bound for all times larger than the mixing time:

$$d_{\text{TV}}(t) \leq \exp(-t/t_{\text{mix}}) \quad (\text{for } t > t_{\text{mix}}), \quad [52]$$

where we define $t_{\text{mix}} = t_{\text{mix}}(1/(2\epsilon))$. The mixing time t_{mix} is a non-asymptotic timescale with a strict inequality for finite times given by Eq. [52]. Importantly, the mixing time can be larger than the inverse gap (in the SSEP, for example $t_{\text{mix}} \sim N^3 \log N$, whereas the inverse gap scales as $t_{\text{rel}} \sim N^3$). This insight is at the basis of the modern theory of Markov chains (25, 35).

However, for asymptotically large times the worst-case distance approaches zero as

$$\lim_{t \rightarrow \infty} d_{\text{TV}}(t)^{1/t} = \lambda^*, \quad [53]$$

where λ^* is the largest absolute value of transition matrix eigenvalues different from $\lambda_1 = 1$ (see Ref. (35, eq. (12.37))). Defining the spectral gap by $\gamma^* = -\ln(\lambda^*)$ and the relaxation time as $t_{\text{rel}} = 1/\gamma^*$, one then has an asymptotic expression

$$d_{\text{TV}} \sim \exp(-\gamma^* t) \quad (\text{for } t \rightarrow \infty). \quad [54]$$

In the SSEP, for example, the mixing time scales more slowly than the relaxation time. This leads to a sudden collapse of d_{TV} (on a time scale t_{mix}), as it switches over from a slow decay on the mixing-time scale (see Eq. [52]) to a faster decay on the relaxation-time scale $t_{\text{rel}} = 1/\gamma^*$.

The relaxation time remains of relevance in equilibrium (rather than only for the asymptotic approach to equilibrium). For reversible Markov chains, one has

$$\text{Var}_\pi P^t g \leq \text{Var}_\pi g \exp(-\lambda_1 t). \quad [55]$$

where g is an arbitrary function on the sample space.

Example transition matrices. For concreteness, we provide examples for transition matrices for the standard and the lifted random walks, as well as the SSEP and its liftings, the TASEP and the lifted TASEP.

Random-walk transition matrices (examples). Here, we give the transition matrices of the random walk for $L = 4$ sites, in the basis:

$$1 \equiv \begin{array}{|c|c|c|c|} \hline \bullet & & & \\ \hline \end{array} \quad 2 \equiv \begin{array}{|c|c|c|c|} \hline & \bullet & & \\ \hline \end{array} \quad 3 \equiv \begin{array}{|c|c|c|c|} \hline & & \bullet & \\ \hline \end{array} \quad 4 \equiv \begin{array}{|c|c|c|c|} \hline & & & \bullet \\ \hline \end{array}.$$

With hard-wall boundary conditions, the case discussed in the main text, we have

$$P_{\text{walls}}^{\text{RW}} = \frac{1}{2} \begin{bmatrix} 1 & 1 & \cdot & \cdot \\ 1 & \cdot & 1 & \cdot \\ \cdot & 1 & \cdot & 1 \\ \cdot & \cdot & 1 & 1 \end{bmatrix}. \quad [56]$$

Here and in the following the ‘‘ \cdot ’’s stand for zeros. This transition matrix is irreducible and aperiodic by virtue of the presence of diagonal terms. It is doubly stochastic (each of its rows and of its columns sum to one), so that the steady state is the equal-probability mixture. As P^{RW} is symmetric and doubly stochastic the associated process is reversible.

Lifted-random-walk transition matrix (example). In the basis

$$\begin{aligned} 1 &\equiv \begin{array}{|c|c|c|c|} \hline \bullet & & & \\ \hline \end{array} & 3 &\equiv \begin{array}{|c|c|c|c|} \hline & \bullet & & \\ \hline \end{array} & 5 &\equiv \begin{array}{|c|c|c|c|} \hline & & \bullet & \\ \hline \end{array} & 7 &\equiv \begin{array}{|c|c|c|c|} \hline & & & \bullet \\ \hline \end{array} \\ 2 &\equiv \begin{array}{|c|c|c|c|} \hline & \bullet & & \\ \hline \end{array} & 4 &\equiv \begin{array}{|c|c|c|c|} \hline & & \bullet & \\ \hline \end{array} & 6 &\equiv \begin{array}{|c|c|c|c|} \hline & & & \bullet \\ \hline \end{array} & 8 &\equiv \begin{array}{|c|c|c|c|} \hline \bullet & & & \\ \hline \end{array}, \end{aligned} \quad [57]$$

the transition matrix of the lifted random walk with hard-wall boundary conditions reads

$$P_{\text{walls}}^{\text{LRW}} = \begin{bmatrix} \cdot & \cdot & \bar{\alpha} & \alpha & \cdot & \cdot & \cdot & \cdot & \cdot \\ \bar{\alpha} & \alpha & \cdot & \cdot & \cdot & \cdot & \cdot & \cdot & \cdot \\ \alpha & \bar{\alpha} & \cdot & \cdot & \cdot & \cdot & \cdot & \cdot & \cdot \\ \cdot & \cdot & \alpha & \bar{\alpha} & \cdot & \cdot & \cdot & \bar{\alpha} & \alpha \\ \cdot & \cdot & \cdot & \cdot & \cdot & \cdot & \cdot & \cdot & \cdot \\ \cdot & \cdot & \cdot & \cdot & \alpha & \bar{\alpha} & \cdot & \cdot & \cdot \\ \cdot & \cdot & \cdot & \cdot & \cdot & \cdot & \alpha & \bar{\alpha} & \cdot \end{bmatrix}.$$

where $\bar{\alpha} = 1 - \alpha$. It is again doubly stochastic, so that the steady state is the equal-probability mixture. As required by Eq. [49], its 2×2 blocks sum up to the corresponding single entries in $P_{\text{walls}}^{\text{RW}}$.

SSEP transition matrices (examples). For the SSEP with two particles on four sites, we use the basis

$$\begin{aligned} 1 &\equiv \begin{array}{|c|c|c|c|} \hline \bullet & \bullet & & \\ \hline \end{array} & 2 &\equiv \begin{array}{|c|c|c|c|} \hline \bullet & & \bullet & \\ \hline \end{array} & 3 &\equiv \begin{array}{|c|c|c|c|} \hline \bullet & & & \bullet \\ \hline \end{array} \\ 4 &\equiv \begin{array}{|c|c|c|c|} \hline \bullet & \bullet & \bullet & \\ \hline \end{array} & 5 &\equiv \begin{array}{|c|c|c|c|} \hline \bullet & \bullet & & \bullet \\ \hline \end{array} & 6 &\equiv \begin{array}{|c|c|c|c|} \hline & & \bullet & \bullet \\ \hline \end{array}. \end{aligned} \quad [58]$$

With periodic boundary conditions, the transition matrix of the SSEP with periodic boundary conditions is

$$P_{\text{pbc}}^{\text{SSEP}} = \frac{1}{4} \begin{bmatrix} 2 & 1 & \cdot & \cdot & 1 & \cdot \\ 1 & \cdot & 1 & 1 & \cdot & 1 \\ \cdot & 1 & 2 & \cdot & 1 & \cdot \\ \cdot & \cdot & \cdot & 2 & 1 & \cdot \\ 1 & \cdot & 1 & 1 & \cdot & 1 \\ \cdot & 1 & \cdot & \cdot & 1 & 2 \end{bmatrix} \quad [59]$$

while for hard-wall boundary conditions one has instead

$$P_{\text{walls}}^{\text{SSEP}} = \frac{1}{4} \begin{bmatrix} 3 & 1 & \cdot & \cdot & \cdot & \cdot \\ 1 & 1 & 1 & 1 & \cdot & \cdot \\ \cdot & 1 & 2 & \cdot & 1 & \cdot \\ \cdot & \cdot & \cdot & 2 & 1 & \cdot \\ \cdot & \cdot & 1 & 1 & 1 & 1 \\ \cdot & \cdot & \cdot & \cdot & 1 & 3 \end{bmatrix}. \quad [60]$$

Both these transition matrices are doubly stochastic, so that in both cases the steady state is the equal-probability mixture. Reversibility again follows from the fact that the transition matrices are doubly stochastic and symmetric.

TASEP transition matrix (example). We first discuss the ‘‘bi-directional’’ TASEP for two particles on four sites in the following basis of $2 \binom{4}{2} = 12$ configurations, twice as many as for the SSEP:

$$\begin{aligned} 1 &\equiv \begin{array}{|c|c|c|c|} \hline \bullet & \bullet & & \\ \hline \end{array} & 2 &\equiv \begin{array}{|c|c|c|c|} \hline \bullet & \bullet & & \\ \hline \end{array} \\ 3 &\equiv \begin{array}{|c|c|c|c|} \hline \bullet & \bullet & & \\ \hline \end{array} & 4 &\equiv \begin{array}{|c|c|c|c|} \hline \bullet & \bullet & & \\ \hline \end{array} \\ \vdots & & & \vdots \\ 11 &\equiv \begin{array}{|c|c|c|c|} \hline & & \bullet & \bullet \\ \hline \end{array} & 12 &\equiv \begin{array}{|c|c|c|c|} \hline & & \bullet & \bullet \\ \hline \end{array} \end{aligned} \quad [61]$$

The bi-directional TASEP rejects moves that violate the exclusion condition (see first row of Eq. [8]), but changes the overall direction upon collision with a wall (more precisely, attempting to move the rightmost particle in configuration ‘‘2’’ leads to ‘‘2’’, while moving the leftmost particle leads to ‘‘1’’). This gives the following transition matrix

$$P_{\text{walls}}^{\text{TASEP}} = \frac{1}{2} \begin{bmatrix} 1 & \cdot & 1 & \cdot & \cdot & \cdot & \cdot & \cdot & \cdot & \cdot & \cdot & \cdot \\ 1 & 1 & \cdot & \cdot & \cdot & \cdot & \cdot & \cdot & \cdot & \cdot & \cdot & \cdot \\ \cdot & \cdot & \cdot & \cdot & 1 & \cdot & 1 & \cdot & \cdot & \cdot & \cdot & \cdot \\ \cdot & 1 & 1 & \cdot & \cdot & \cdot & \cdot & \cdot & \cdot & \cdot & \cdot & \cdot \\ \cdot & \cdot & \cdot & \cdot & \cdot & 1 & \cdot & \cdot & 1 & \cdot & \cdot & \cdot \\ \cdot & \cdot & \cdot & \cdot & \cdot & \cdot & \cdot & 1 & \cdot & \cdot & \cdot & \cdot \\ \cdot & \cdot & \cdot & \cdot & \cdot & \cdot & \cdot & \cdot & \cdot & 1 & 1 & \cdot \\ \cdot & \cdot & \cdot & \cdot & \cdot & \cdot & \cdot & \cdot & \cdot & \cdot & \cdot & 1 \\ \cdot & \cdot & \cdot & \cdot & \cdot & \cdot & \cdot & \cdot & \cdot & \cdot & 1 & 1 \\ \cdot & \cdot & \cdot & \cdot & \cdot & \cdot & \cdot & \cdot & \cdot & \cdot & 1 & 1 \end{bmatrix}. \quad [62]$$

While $P_{\text{walls}}^{\text{TASEP}}$ is doubly stochastic and concomitantly the steady state is the equal-probability mixture, it is non-symmetric and the

TASEP is thus clearly non-reversible. The 2×2 blocks in Eq. [62] again sum up to the corresponding entries of $P_{\text{walls}}^{\text{SSEP}}$ (see Eq. [60]) and the bi-directional TASEP is thus a lifting of the SSEP.

The transition matrix of the bi-directional TASEP with periodic boundary conditions can be written as a lifting of the SSEP, in the basis of Eq. [61], with appropriate flipping probabilities between the forward and backward sectors. The periodic boundary conditions allow one to restrict one’s attention to the forward sector. For two particles on four sites, in the ‘‘forward’’ basis equivalent to that of Eq. [58], this yields:

$$P_{\text{pbc}}^{\text{TASEP}} = \frac{1}{2} \begin{bmatrix} 1 & 1 & \cdot & \cdot & \cdot & \cdot \\ \cdot & \cdot & 1 & 1 & \cdot & \cdot \\ \cdot & \cdot & \cdot & 1 & 1 & \cdot \\ \cdot & \cdot & \cdot & \cdot & 1 & 1 \\ 1 & \cdot & \cdot & \cdot & \cdot & 1 \\ \cdot & 1 & \cdot & \cdot & \cdot & 1 \end{bmatrix}. \quad [63]$$

This transition matrix is irreducible and aperiodic because of the presence of non-zero diagonal elements. It is an incomplete lifting of the SSEP, because of the absence of backward moves. Nevertheless, as a doubly stochastic matrix, its steady state is the equal-probability mixture.

Lifted TASEP transition matrix (example). For simplicity, we consider the transition matrix of the lifted TASEP with periodic boundary conditions only in the forward sector. This leaves us with $N \binom{L}{N}$ configurations. For two particles on four sites we have

$$\begin{aligned} 1 &\equiv \begin{array}{|c|c|c|c|} \hline \bullet & \bullet & & \\ \hline \end{array} & 2 &\equiv \begin{array}{|c|c|c|c|} \hline \bullet & \bullet & & \\ \hline \end{array} & 3 &\equiv \begin{array}{|c|c|c|c|} \hline \bullet & & \bullet & \\ \hline \end{array} & 4 &\equiv \begin{array}{|c|c|c|c|} \hline \bullet & & & \bullet \\ \hline \end{array} \\ 5 &\equiv \begin{array}{|c|c|c|c|} \hline \bullet & \bullet & & \\ \hline \end{array} & 6 &\equiv \begin{array}{|c|c|c|c|} \hline \bullet & \bullet & & \\ \hline \end{array} & 7 &\equiv \begin{array}{|c|c|c|c|} \hline \bullet & & \bullet & \\ \hline \end{array} & 8 &\equiv \begin{array}{|c|c|c|c|} \hline \bullet & & & \bullet \\ \hline \end{array} \\ 9 &\equiv \begin{array}{|c|c|c|c|} \hline \bullet & \bullet & & \\ \hline \end{array} & 10 &\equiv \begin{array}{|c|c|c|c|} \hline \bullet & \bullet & & \\ \hline \end{array} & 11 &\equiv \begin{array}{|c|c|c|c|} \hline & & \bullet & \bullet \\ \hline \end{array} & 12 &\equiv \begin{array}{|c|c|c|c|} \hline & & \bullet & \bullet \\ \hline \end{array}. \end{aligned}$$

In this basis, the transition matrix of the lifted TASEP follows from Eqs [15] and [16] to be

$$P^{\text{L-T}} = \begin{bmatrix} \alpha & \bar{\alpha} & \cdot & \cdot & \cdot & \cdot & \cdot & \cdot & \cdot & \cdot & \cdot & \cdot \\ \cdot & \cdot & \alpha & \bar{\alpha} & \cdot & \cdot & \cdot & \cdot & \cdot & \cdot & \cdot & \cdot \\ \cdot & \cdot & \cdot & \cdot & \alpha & \bar{\alpha} & \cdot & \cdot & \cdot & \cdot & \cdot & \cdot \\ \cdot & \cdot & \cdot & \cdot & \cdot & \cdot & \alpha & \bar{\alpha} & \cdot & \cdot & \cdot & \cdot \\ \cdot & \cdot & \cdot & \cdot & \cdot & \cdot & \cdot & \cdot & \alpha & \bar{\alpha} & \cdot & \cdot \\ \cdot & \cdot & \cdot & \cdot & \cdot & \cdot & \cdot & \cdot & \cdot & \cdot & \alpha & \bar{\alpha} \\ \cdot & \cdot & \cdot & \cdot & \cdot & \cdot & \cdot & \cdot & \cdot & \cdot & \cdot & \alpha \\ \bar{\alpha} & \alpha & \cdot & \cdot & \cdot & \cdot & \cdot & \cdot & \cdot & \cdot & \cdot & \cdot \\ \cdot & \cdot & \bar{\alpha} & \alpha & \cdot & \cdot & \cdot & \cdot & \cdot & \cdot & \cdot & \cdot \end{bmatrix}, \quad [64]$$

where $\bar{\alpha} = \alpha - 1$. $P^{\text{L-T}}$ is doubly stochastic (so that its steady state is the equal-probability mixture), irreducible and is aperiodic (as a result of the presence of non-zero diagonal elements). The transition matrix $P^{\text{L-T}}$ can be partitioned into 2×2 blocks that sum up to the analogous elements of $P_{\text{pbc}}^{\text{TASEP}}$, as required for a lifting.

Three-particle Bethe ansatz (example). For concreteness, we present a step-by-step derivation of the Bethe ansatz equations of the lifted TASEP for $N = 3$ particles on an L -site lattice with periodic boundary conditions. The left eigenvalue equations for the transition matrix, in the case where all three particles are well separated ($j < k - 1$, $k < l - 1$), take the form

$$\begin{aligned} E\psi_{\{\vec{j},k,l\}} &= \bar{\alpha}\psi_{\{\vec{j}-\vec{1},k,l\}} + \alpha\psi_{\{\vec{j},\vec{k}-\vec{1},l\}}, \\ E\psi_{\{\vec{j},\vec{k},l\}} &= \bar{\alpha}\psi_{\{\vec{j},\vec{k}-\vec{1},l\}} + \alpha\psi_{\{\vec{j},k,\vec{l}-\vec{1}\}}, \\ E\psi_{\{\vec{j},k,\vec{l}\}} &= \bar{\alpha}\psi_{\{\vec{j},k,\vec{l}-\vec{1}\}} + \alpha\psi_{\{\vec{j}-\vec{1},k,l\}}. \end{aligned} \quad [65]$$

The Bethe ansatz for ψ then reads

$$\begin{aligned} \psi_{\{\vec{j},k,l\}} &= A_{\bullet\circ\circ} z_1^j z_2^k z_3^l + B_{\circ\bullet\circ} z_1^j z_2^k z_3^l + \dots + F_{\circ\circ\bullet} z_1^j z_2^k z_3^l, \\ \psi_{\{\vec{j},\vec{k},l\}} &= A_{\circ\bullet\circ} z_1^j z_2^k z_3^l + B_{\circ\circ\bullet} z_1^j z_2^k z_3^l + \dots + F_{\circ\circ\bullet} z_1^j z_2^k z_3^l, \\ \psi_{\{\vec{j},k,\vec{l}\}} &= A_{\circ\circ\bullet} z_1^j z_2^k z_3^l + B_{\circ\circ\bullet} z_1^j z_2^k z_3^l + \dots + F_{\circ\circ\bullet} z_1^j z_2^k z_3^l. \end{aligned} \quad [66]$$

The three sectors $\{\bullet\circ\circ\}$, $\{\circ\bullet\circ\}$ and $\{\circ\circ\bullet\}$ correspond to the position of the active particle, while the six coefficients A, B, \dots, F

correspond to the permutations of the indices i, j, k . Inserting Eq. [66] into Eq. [65] and comparing coefficients yields

$$\begin{aligned} \left(E - \frac{\bar{\alpha}}{z_1}\right) A_{\bullet\circ\circ} &= \frac{\alpha}{z_2} A_{\circ\bullet\circ}; \left(E - \frac{\bar{\alpha}}{z_1}\right) B_{\bullet\circ\circ} = \frac{\alpha}{z_3} B_{\circ\bullet\circ}; \dots \\ \left(E - \frac{\bar{\alpha}}{z_2}\right) A_{\circ\bullet\circ} &= \frac{\alpha}{z_3} A_{\circ\circ\bullet}; \left(E - \frac{\bar{\alpha}}{z_2}\right) B_{\circ\bullet\circ} = \frac{\alpha}{z_2} B_{\circ\circ\bullet}; \dots \\ \left(E - \frac{\bar{\alpha}}{z_3}\right) A_{\circ\circ\bullet} &= \frac{\alpha}{z_1} A_{\bullet\circ\circ}; \left(E - \frac{\bar{\alpha}}{z_3}\right) B_{\circ\circ\bullet} = \frac{\alpha}{z_1} B_{\bullet\circ\circ}; \dots \end{aligned} \quad [67]$$

Multiplying these equations for each of the A, B, \dots, F coefficients yields

$$\prod_{a=1}^3 \left(E - \frac{\bar{\alpha}}{z_a}\right) = \frac{\alpha^3}{z_1 z_2 z_3}, \quad [68]$$

which is identical for $N = 3$ to the second expression in Eq. [34].

Next, we now consider the eigenvalue equations in the case when two particles are on neighboring sites and the third particle is detached:

$$\begin{aligned} E\psi_{\{\bar{k}-1, k, l\}} &= \bar{\alpha}\psi_{\{\bar{k}-2, k, l\}} + \alpha\psi_{\{\bar{k}-1, k, l\}}, \\ E\psi_{\{k-1, \bar{k}, l\}} &= \bar{\alpha}\psi_{\{\bar{k}-1, k, l\}} + \alpha\psi_{\{k-1, k, \bar{l}-1\}}, \\ E\psi_{\{j, \bar{l}-1, l\}} &= \bar{\alpha}\psi_{\{j, \bar{l}-2, l\}} + \alpha\psi_{\{j, \bar{l}-1, l\}}, \\ E\psi_{\{j, l-1, \bar{l}\}} &= \bar{\alpha}\psi_{\{j, \bar{l}-1, l\}} + \alpha\psi_{\{j, \bar{l}-1, l-1\}}. \end{aligned} \quad [69]$$

Substituting Eq. [66] into Eq. [69] and comparing coefficients gives

$$\begin{aligned} \frac{A_{\bullet\circ\circ}}{C_{\bullet\circ\circ}} &= S_{12}; \frac{B_{\bullet\circ\circ}}{D_{\bullet\circ\circ}} = S_{13}; \frac{E_{\bullet\circ\circ}}{F_{\bullet\circ\circ}} = S_{23}, \\ \frac{A_{\circ\bullet\circ}}{B_{\circ\bullet\circ}} &= S_{23}; \frac{C_{\circ\bullet\circ}}{E_{\circ\bullet\circ}} = S_{13}; \frac{F_{\circ\bullet\circ}}{D_{\circ\bullet\circ}} = S_{21}, \end{aligned} \quad [70]$$

where

$$S_{kl} = -\frac{z_k}{z_l} \frac{E - \alpha - \bar{\alpha}/z_l}{E - \alpha - \bar{\alpha}/z_k}. \quad [71]$$

Proceeding analogously with the second and third lines in Eq. [69] yields:

$$\begin{aligned} E \left(\frac{A_{\circ\circ\bullet} + B_{\circ\circ\bullet}}{z_2 + z_3} \right) - \bar{\alpha} \left(\frac{A_{\circ\circ\circ} + B_{\circ\circ\circ}}{z_2 + z_1} \right) - \alpha \left(\frac{A_{\bullet\circ\circ} + B_{\bullet\circ\circ}}{z_1 z_2 + z_3 z_1} \right) &= 0, \\ E \left(\frac{A_{\circ\circ\circ} + C_{\circ\circ\circ}}{z_1 + z_2} \right) - \bar{\alpha} \left(\frac{A_{\bullet\circ\circ} + C_{\bullet\circ\circ}}{z_1 + z_2} \right) - \alpha \left(\frac{A_{\circ\circ\bullet} + C_{\circ\circ\bullet}}{z_3 z_1 + z_3 z_2} \right) &= 0, \end{aligned}$$

and five additional equations that start with B, \dots, F . The solution to these conditions is:

$$\begin{aligned} B_{\bullet\circ\circ} &= \frac{z_2}{z_3} S_{32} A_{\bullet\circ\circ}, \\ C_{\bullet\circ\circ} &= S_{21} A_{\bullet\circ\circ}, \\ D_{\bullet\circ\circ} &= \frac{z_2}{z_3} S_{31} S_{32} A_{\bullet\circ\circ}, \\ E_{\bullet\circ\circ} &= \frac{z_1}{z_3} S_{21} S_{31} A_{\bullet\circ\circ}, \\ F_{\bullet\circ\circ} &= \frac{z_1}{z_3} S_{21} S_{31} S_{32} A_{\bullet\circ\circ}, \end{aligned} \quad [72]$$

which fixes all amplitudes B, \dots, F in terms of A .

Finally, the sector with three adjacent occupied sites yields the following eigenvalue equations:

$$E\psi_{\{\bar{j}, j+1, j+2\}} = \bar{\alpha}\psi_{\{\bar{j}-1, j+1, j+2\}} + \alpha\psi_{\{\bar{j}, j+1, j+2\}}, \quad [73]$$

$$E\psi_{\{j, \bar{j}+1, j+2\}} = \bar{\alpha}\psi_{\{\bar{j}, j+1, j+2\}} + \alpha\psi_{\{j, \bar{j}+1, j+2\}}, \quad [74]$$

$$E\psi_{\{j, j+1, \bar{j}+2\}} = \bar{\alpha}\psi_{\{j, \bar{j}+1, j+2\}} + \alpha\psi_{\{\bar{j}-1, j+1, j+2\}}, \quad [75]$$

Of these equations, only Eq. [74] leads to a new relation:

$$\begin{aligned} \{[E - \alpha]A_{\circ\circ\bullet} - \bar{\alpha}A_{\bullet\circ\circ}\} \frac{z_3}{z_1} + \{[E - \alpha]B_{\circ\circ\bullet} - \bar{\alpha}B_{\bullet\circ\circ}\} \frac{z_2}{z_1} + \\ \{[E - \alpha]C_{\circ\circ\circ} - \bar{\alpha}C_{\bullet\circ\circ}\} \frac{z_3}{z_2} + \{[E - \alpha]D_{\circ\circ\circ} - \bar{\alpha}D_{\bullet\circ\circ}\} \frac{z_2}{z_1} + \\ \{[E - \alpha]E_{\circ\circ\circ} - \bar{\alpha}E_{\bullet\circ\circ}\} \frac{z_1}{z_2} + \{[E - \alpha]F_{\circ\circ\circ} - \bar{\alpha}F_{\bullet\circ\circ}\} \frac{z_1}{z_3} = 0. \end{aligned}$$

Crucially, this condition is identically satisfied as a consequence of Eqs [67] and [72].

The periodic boundary conditions:

$$\psi_{\{j, k, \bar{l}\}} = \psi_{\{\bar{l}, j, k\}}, \quad [76]$$

give the following relations for the spectral parameters $\{z_1, z_2, z_3\}$:

$$z_a^{L-1} = \left(\frac{E - \bar{\alpha}/z_a}{\alpha} \right) \prod_{b \neq a=1}^3 T(z_a, z_b), \quad a = 1, 2, 3, \quad [77]$$

where

$$T(z_a, z_b) = -\frac{E - \alpha - \bar{\alpha}/z_b}{E - \alpha - \bar{\alpha}/z_a} \quad [78]$$

(cf Eq. [27]).

Representation as a non-Hermitian quantum spin chain. We may consider the transition matrix to induce a continuous time evolution, which then can be cast in the form of an imaginary-time Schrödinger equation (32). To do so we define three basis states $|a\rangle_j$ with $a = 0, 1, 2$ on each site of the lattice and a basis of operators acting on them

$$E_j^{ab} = |a\rangle_j \langle b|, \quad a, b \in \{0, 1, 2\}. \quad [79]$$

The probability distributions of the stochastic process give rise to states by the map

$$|\psi\rangle = \sum_{j_1 < j_2 < \dots < j_N} \sum_{a=1}^N \psi_a(j) E_{j_1}^{\sigma_1 0} E_{j_2}^{\sigma_2 0} \dots E_{j_N}^{\sigma_N 0} |0\rangle. \quad [80]$$

The master equation takes the form of an imaginary-time Schrödinger equation

$$\frac{d}{dt} |P(t)\rangle = H |P(t)\rangle, \quad [81]$$

where the ‘‘Hamiltonian’’ is given by

$$H = \sum_{j=1}^N [\bar{\alpha} + \alpha P_{12}] [E_j^{02} E_{j+1}^{20} + E_j^{12} E_{j+1}^{21}]. \quad [82]$$

Here P_{12} is a non-local operator that permutes the active particle with the regular particle preceding it:

$$P_{12} = \sum_{k < j} E_k^{21} \prod_{\ell=k+1}^{j-1} E_\ell^{00} E_j^{12} + \sum_{j < k} \prod_{\ell=1}^{j-1} E_\ell^{00} E_j^{12} E_k^{21} \prod_{\ell=k+1}^L E_\ell^{00}. \quad [83]$$

ACKNOWLEDGMENTS. This work was supported in part by the EPSRC under grant EP/S020527/1 (FHLE) and the Alexander-von-Humboldt foundation (WK). We are grateful to A. C. Maggs, C. Monthus, G. Robichon, and M. Staudacher for helpful discussions.

1. N. Metropolis, A. W. Rosenbluth, M. N. Rosenbluth, A. H. Teller, and E. Teller. Equation of State Calculations by Fast Computing Machines. *J. Chem. Phys.*, 21:1087–1092, 1953. . URL <https://doi.org/10.1093/tpami.1984.4.767596>.
2. R. J. Glauber. Time-Dependent Statistics of the Ising Model. *J. Math. Phys.*, 4:294–307, 1963. . URL [https://doi.org/10.1016/0001-8708\(70\)90034-4](https://doi.org/10.1016/0001-8708(70)90034-4).
3. M. Creutz. Monte Carlo study of quantized SU(2) gauge theory. *Phys. Rev. D*, 21:2308–2315, 1980. . URL <https://link.aps.org/doi/10.1103/PhysRevD.21.2308>.
4. S. Geman and D. Geman. Stochastic Relaxation, Gibbs Distributions, and the Bayesian Restoration of Images. *IEEE Trans. Pattern Anal. Mach. Intell.*, PAMI-6(6):721–741, 1984. . URL <https://doi.org/10.1109/tpami.1984.4.767596>.
5. P. Diaconis, S. Holmes, and R. M. Neal. Analysis of a nonreversible Markov chain sampler. *Ann. Appl. Probab.*, 10:726–752, 2000. . URL <https://doi.org/10.1214/15-aop1053>.
6. F. Chen, L. Lovász, and I. Pak. Lifting Markov Chains to Speed up Mixing. *Proceedings of the 17th Annual ACM Symposium on Theory of Computing*, page 275, 1999.
7. F. Spitzer. Interaction of Markov processes. *Adv. Math.*, 5(2):246–290, 1970. . URL [https://doi.org/10.1016/0001-8708\(70\)90034-4](https://doi.org/10.1016/0001-8708(70)90034-4).
8. H. Lacoïn. The cutoff profile for the simple exclusion process on the circle. *Ann. Probab.*, 44(5):3399–3430, 2016. . URL <https://doi.org/10.1214/15-aop1053>.
9. H. Lacoïn. The simple exclusion process on the circle has a diffusive cutoff window. *Ann. Inst. H. Poincaré Probab. Statist.*, 53(3):1402–1437, 2017. . URL <https://doi.org/10.1103/PhysRevLett.119.240603>.
10. S. C. Kapfer and W. Krauth. Irreversible Local Markov Chains with Rapid Convergence towards Equilibrium. *Phys. Rev. Lett.*, 119:240603, 2017. . URL <https://doi.org/10.1103/PhysRevLett.119.240603>.
11. Z. Lei, W. Krauth, and A. C. Maggs. Event-chain Monte Carlo with factor fields. *Phys. Rev. E*, 99(4), 2019. . URL <https://doi.org/10.1103/physreve.99.043301>.

12. E. P. Bernard, W. Krauth, and D. B. Wilson. Event-chain Monte Carlo algorithms for hard-sphere systems. *Phys. Rev. E*, 80:056704, 2009. . URL <http://link.aps.org/doi/10.1103/PhysRevE.80.056704>.
13. A. C. Maggs and W. Krauth. Large-scale dynamics of event-chain Monte Carlo. *Physical Review E*, 105(1), January 2022. . URL <https://doi.org/10.1103/physreve.105.015309>.
14. E. A. J. F. Peters and G. de With. Rejection-free Monte Carlo sampling for general potentials. *Phys. Rev. E*, 85:026703, 2012. . URL <http://link.aps.org/doi/10.1103/PhysRevE.85.026703>.
15. M. Michel, S. C. Kapfer, and W. Krauth. Generalized event-chain Monte Carlo: Constructing rejection-free global-balance algorithms from infinitesimal steps. *J. Chem. Phys.*, 140(5): 054116, 2014. .
16. E. P. Bernard and W. Krauth. Two-Step Melting in Two Dimensions: First-Order Liquid-Hexatic Transition. *Phys. Rev. Lett.*, 107:155704, 2011. . URL <http://link.aps.org/doi/10.1103/PhysRevLett.107.155704>.
17. T. A. Kampmann, D. Müller, L. P. Weise, C. F. Vorsmann, and J. Kierfeld. Event-Chain Monte-Carlo Simulations of Dense Soft Matter Systems. *Front. Phys.*, 9:96, 2021. . URL <https://doi.org/10.3389/fphy.2021.635886>.
18. M. F. Faulkner, L. Qin, A. C. Maggs, and W. Krauth. All-atom computations with irreversible Markov chains. *J. Chem. Phys.*, 149(6):064113, 2018. . URL <https://doi.org/10.1063/1.5036638>.
19. L.-H. Gwa and H. Spohn. Six-vertex model, roughened surfaces, and an asymmetric spin Hamiltonian. *Phys. Rev. Lett.*, 68:725–728, 1992. . URL <https://link.aps.org/doi/10.1103/PhysRevLett.68.725>.
20. L.-H. Gwa and H. Spohn. Bethe solution for the dynamical-scaling exponent of the noisy Burgers equation. *Phys. Rev. A*, 46:844–854, 1992. . URL <https://link.aps.org/doi/10.1103/PhysRevA.46.844>.
21. D. Kim. Bethe ansatz solution for crossover scaling functions of the asymmetric XXZ chain and the Kardar-Parisi-Zhang-type growth model. *Phys. Rev. E*, 52:3512–3524, 1995. . URL <https://link.aps.org/doi/10.1103/PhysRevE.52.3512>.
22. B. Derrida. An exactly soluble non-equilibrium system: the asymmetric simple exclusion process. *Physics Reports*, 301(1-3):65–83, 1998.
23. G. M. Schütz. Exactly solvable models for many-body systems far from equilibrium. In *Phase transitions and critical phenomena*, volume 19, pages 1–251. Elsevier, 2001.
24. T. Chou, K. Mallick, and R. K. P. Zia. Non-equilibrium statistical mechanics: from a paradigmatic model to biological transport. *Rep. Prog. Phys.*, 74(11):116601, 2011. URL <http://stacks.iop.org/0034-4885/74/i=11/a=116601>.
25. D. Aldous and P. Diaconis. Shuffling Cards and Stopping Times. *Am. Math. Mon.*, 93(5): 333–348, 1986. ISSN 00029890, 19300972. URL <http://www.jstor.org/stable/2323590>.
26. D. Dhar. An exactly solved model for interfacial growth. *Phase Transitions*, 9(1):51, 1987. .
27. J. Baik and Z. Liu. TASEP on a Ring in Sub-relaxation Time Scale. *J. Stat. Phys.*, 165(6): 1051–1085, 2016. ISSN 1572-9613. . URL <http://dx.doi.org/10.1007/s10955-016-1665-y>.
28. M. Kardar, G. Parisi, and Y.-C. Zhang. Dynamic Scaling of Growing Interfaces. *Phys. Rev. Lett.*, 56:889–892, 1986. . URL <https://link.aps.org/doi/10.1103/PhysRevLett.56.889>.
29. B. Derrida and M. R. Evans. Bethe ansatz solution for a defect particle in the asymmetric exclusion process. *J. Phys. A: Math. Gen.*, 32(26):4833–4850, 1999. . URL <https://doi.org/10.1088%2F0305-4470%2F32%2F26%2F303>.
30. Z. Lei and W. Krauth. Irreversible Markov chains in spin models: Topological excitations. *EPL*, 121:10008, 2018.
31. A. Sokal. *Monte Carlo Methods in Statistical Mechanics: Foundations and New Algorithms*, pages 131–192. Springer US, 1997. ISBN 978-1-4899-0319-8. . URL https://doi.org/10.1007/978-1-4899-0319-8_6.
32. F. C. Alcaraz, M. Droz, M. Henkel, and V. Rittenberg. Reaction-diffusion processes, critical dynamics, and quantum chains. *Ann. Phys. (N. Y.)*, 230(2):250–302, 1994.
33. S. F. Edwards and D. R. Wilkinson. The surface statistics of a granular aggregate. *Proc. R. Soc. A*, 381(1780):17–31, 1982.
34. Pietro Caputo, Thomas Liggett, and Thomas Richthammer. Proof of Aldous' spectral gap conjecture. *Journal of the American Mathematical Society*, 23(3):831–851, 2010. . URL <https://doi.org/10.1090/s0894-0347-10-00659-4>.
35. D. A. Levin and Y. Peres. *Markov Chains and Mixing Times, Second Edition*. American Mathematical Society, 2017.
36. W. Krauth. Event-Chain Monte Carlo: Foundations, Applications, and Prospects. *Front. Phys.*, 9:229, 2021. ISSN 2296-424X. . URL <https://www.frontiersin.org/article/10.3389/fphy.2021.663457>.
37. J. de Gier and F. H. L. Essler. Bethe Ansatz Solution of the Asymmetric Exclusion Process with Open Boundaries. *Phys. Rev. Lett.*, 95:240601, 2005. . URL <https://link.aps.org/doi/10.1103/PhysRevLett.95.240601>.
38. J. de Gier and F. H. L. Essler. Exact spectral gaps of the asymmetric exclusion process with open boundaries. *J. Stat. Mech.*, 2006(12):P12011, 2006. . URL <https://iopscience.iop.org/article/10.1088/1742-5468/2006/12/P12011>.
39. J. de Gier and F. H. L. Essler. Slowest relaxation mode of the partially asymmetric exclusion process with open boundaries. *J. Phys. A: Math. Theor.*, 41(48):485002, 2008. . URL <https://doi.org/10.1088%2F1751-8113%2F41%2F48%2F485002>.
40. V. E. Korepin, N. M. Bogoliubov, and A. G. Izergin. *Quantum inverse scattering method and correlation functions*, volume 3. Cambridge University Press, 1997.
41. B. Derrida, M. R. Evans, V. Hakim, and V. Pasquier. Exact solution of a 1D asymmetric exclusion model using a matrix formulation. *J. Phys. A*, 26(7):1493, 1993.